Compact titanium dioxide waveguides with high nonlinearity at telecommunication wavelengths

Guan, Xiaowei; Hu, Hao; Oxenløwe, Leif Katsuo; Frandsen, Lars Hagedorn

Published in:
Optics Express

Link to article, DOI:
10.1364/OE.26.001055

Publication date:
2018

Document Version
Publisher's PDF, also known as Version of record

Research Article | Vol. 26, No. 2 | 22 Jan 2018 | OPTICS EXPRESS 1055
Optics EXPRESS

Compact titanium dioxide waveguides with high nonlinearity at telecommunication wavelengths

XIAOWEI GUAN,* HAO HU, LEIF K. OXENLØWE AND LARS H. FRANDSEN

DTU Fotonik, Department of Photonics Engineering, Technical University of Denmark, 2800 Kgs. Lyngby, Denmark
**xgua@fotonik.dtu.dk*

Abstract: Dense integration of photonic integrated circuits demands waveguides simultaneously fulfilling requirements on compactness, low loss, high nonlinearity, and capabilities for mass production. In this work, titanium dioxide waveguides with a thick core of 380 nm exhibiting a compact mode size (0.43 μm^2) and a low loss (5.4 ± 1 dB/cm) at telecommunication wavelengths around 1550 nm have been fabricated and measured. A microring resonator having a 50 μm radius has been measured to have a loaded quality factor of 53500. Four-wave mixing experiments reveal a nonlinear parameter for the waveguides of 21-34 W^{-1} m^{-1} corresponding to a nonlinear index around 2.3-3.6 x 10^{-18} m^2/W, which results in a wavelength conversion efficiency of −36.2 dB. These performances, together with the potentially simple dispersion engineering to the fabricated waveguides by the post processes, yield a strong promise for the titanium dioxide waveguides applied in photonic integrated circuits, especially for nonlinear implementations.

OCIS codes: (130.3120) Integrated optics devices; (160.3130) Integrated optics materials; (190.4380) Nonlinear optics, four-wave mixing.

References and links

1. R. Nagarajan, C. H. Joyner, R. P. Schneider, J. S. Bostak, T. Butrie, A. G. Dentai, V. G. Dominic, P. W. Evans, M. Kato, M. Kauffman, D. J. H. Lambert, S. K. Mathis, A. Mathur, R. H. Miles, M. L. Mitchell, M. J. Missey, S. Murthy, A. C. Nilsson, F. H. Peters, S. C. Pennypacker, J. L. Pleumeekers, R. A. Salvatore, R. K. Schlenker, R. B. Taylor, M. F. Huan-Shang Tsai, M. F. Van Leeuwen, J. Webjorn, M. Ziari, D. Perkins, J. Singh, S. G. Grubb, M. S. Reffle, D. G. Mehuys, F. A. Kish, and D. F. Welch, "Large-scale photonic integrated circuits," IEEE J. Sel. Top. Quantum Electron. **11**(1), 50–65 (2005).
2. A. Politi, M. J. Cryan, J. G. Rarity, S. Yu, and J. L. O'Brien, "Silica-on-silicon waveguide quantum circuits," Science **320**(5876), 646–649 (2008).
3. T. J. Kippenberg, R. Holzwarth, and S. A. Diddams, "Microresonator-based optical frequency combs," Science **332**(6029), 555–559 (2011).
4. D. Culemann, A. Knuettel, and E. Voges, "Integrated optical sensor in glass for optical coherence tomography (OCT)," IEEE J. Sel. Top. Quantum Electron. **6**(5), 730–734 (2000).
5. V. D. Nguyen, B. I. Akca, K. Wörhoff, R. M. de Ridder, M. Pollnau, T. G. van Leeuwen, and J. Kalkman, "Spectral domain optical coherence tomography imaging with an integrated optics spectrometer," Opt. Lett. **36**(7), 1293–1295 (2011).
6. X. Fan, I. M. White, S. I. Shopova, H. Zhu, J. D. Suter, and Y. Sun, "Sensitive optical biosensors for unlabeled targets: A review," Anal. Chim. Acta **620**(1-2), 8–26 (2008).
7. Y. Yanagase, S. Suzuki, Y. Kokubun, and S. T. Chu, "Box-like filter response and expansion of FSR by a vertically triple coupled microring resonator filter," J. Lightwave Technol. **20**(8), 1525–1529 (2002).
8. S. Chu, B. Little, W. Pan, T. Kaneko, S. Sato, and Y. Kokubun, "An eight-channel add-drop filter using vertically coupled microring resonators over a cross grid," IEEE Photonics Technol. Lett. **11**(6), 691–693 (1999).
9. B. Little, S. Chu, P. Absil, J. Hryniewicz, F. Johnson, F. Seiferth, D. Gill, V. Van, O. King, and M. Trakalo, "Very high-order microring resonator filters for WDM applications," IEEE Photonics Technol. Lett. **16**(10), 2263–2265 (2004).
10. C. Dragone, C. Edwards, and R. Kistler, "Integrated optics N*N multiplexer on silicon," IEEE Photonics Technol. Lett. **3**(10), 896–899 (1991).
11. D. Dai, J. Wang, and Y. Shi, "Silicon mode (de)multiplexer enabling high capacity photonic networks-on-chip with a single-wavelength-carrier light," Opt. Lett. **38**(9), 1422–1424 (2013).
12. V. R. Almeida, C. A. Barrios, R. R. Panepucci, and M. Lipson, "All-optical control of light on a silicon chip," Nature **431**(7012), 1081–1084 (2004).
13. R. Salem, M. Foster, A. Turner, D. Geraghty, M. Lipson, and A. Gaeta, "Signal regeneration using low-power four-wave mixing on silicon chip," Nat. Photonics **2**(1), 35–38 (2008).
14. H. Fukuda, K. Yamada, T. Shoji, M. Takahashi, T. Tsuchizawa, T. Watanabe, J. Takahashi, and S. Itabashi,

#312922 https://doi.org/10.1364/OE.26.001055
Journal © 2018 Received 7 Nov 2017; revised 22 Dec 2017; accepted 5 Jan 2018; published 10 Jan 2018

Optics EXPRESS

"Four-wave mixing in silicon wire waveguides," Opt. Express **13**(12), 4629–4637 (2005).
15. J. Levy, A. Gondarenko, M. Foster, A. Turner-Foster, A. Gaeta, and M. Lipson, "CMOS-compatible multiple-wavelength oscillator for on-chip optical interconnects," Nat. Photonics **4**(1), 37–40 (2010).
16. J. Li, H. Lee, T. Chen, and K. J. Vahala, "Low-pump-power, low-phase-noise, and microwave to millimeter-wave repetition rate operation in microcombs," Phys. Rev. Lett. **109**(23), 233901 (2012).
17. P. Del'Haye, A. Schliesser, O. Arcizet, T. Wilken, R. Holzwarth, and T. J. Kippenberg, "Optical frequency comb generation from a monolithic microresonator," Nature **450**(7173), 1214–1217 (2007).
18. L. Razzari, D. Duchesne, M. Ferrera, R. Morandotti, S. Chu, B. Little, and D. Moss, "CMOS-compatible integrated optical hyper-parametric oscillator," Nat. Photonics **4**(1), 41–45 (2010).
19. M. Pu, L. Ottaviano, E. Semenova, and K. Yvind, "Efficient frequency comb generation in AlGaAs-on-insulator," Optica **3**(8), 823–826 (2016).
20. J. Leuthold, C. Koos, and W. Freude, "Nonlinear silicon photonics," Nat. Photonics **4**(8), 535–544 (2010).
21. A. R. Johnson, A. S. Mayer, A. Klenner, K. Luke, E. S. Lamb, M. R. E. Lamont, C. Joshi, Y. Okawachi, F. W. Wise, M. Lipson, U. Keller, and A. L. Gaeta, "Octave-spanning coherent supercontinuum generation in a silicon nitride waveguide," Opt. Lett. **40**(21), 5117–5120 (2015).
22. Y. Okawachi, K. Saha, J. S. Levy, Y. H. Wen, M. Lipson, and A. L. Gaeta, "Octave-spanning frequency comb generation in a silicon nitride chip," Opt. Lett. **36**(17), 3398–3400 (2011).
23. D. Moss, R. Morandotti, A. Gaeta, and M. Lipson, "New CMOS-compatible platforms based on silicon nitride and Hydex for nonlinear optics," Nat. Photonics **7**(8), 597–607 (2013).
24. M. Belt, M. Davenport, J. Bowers, and D. Blumenthal, "Ultra-low-loss Ta_2O_5-core/SiO_2-clad planar waveguides on Si substrates," Optica **4**(5), 532–536 (2017).
25. C. Lacava, S. Stankovic, A. Z. Khokhar, T. D. Bucio, F. Y. Gardes, G. T. Reed, D. J. Richardson, and P. Petropoulos, "Si-rich silicon nitride for nonlinear signal processing applications," Sci. Rep. **7**(1), 22 (2017).
26. T. Wang, D. Ng, S. Ng, Y. Toh, A. Chee, G. Chen, Q. Wang, and D. Tan, "Supercontinuum generation in bandgap engineered, back-end CMOS compatible silicon rich nitride waveguides," Laser Photonics Rev. **9**(5), 498–506 (2015).
27. J. W. Choi, G. F. Chen, D. K. Ng, K. J. Ooi, and D. T. Tan, "Wideband nonlinear spectral broadening in ultra-short ultra - silicon rich nitride waveguides," Sci. Rep. **6**(1), 27120 (2016).
28. C. J. Krückel, A. Fülöp, Z. Ye, P. A. Andrekson, and V. Torres-Company, "Optical bandgap engineering in nonlinear silicon nitride waveguides," Opt. Express **25**(13), 15370–15380 (2017).
29. C. J. Krückel, A. Fülöp, T. Klintberg, J. Bengtsson, P. A. Andrekson, and V. Torres-Company, "Linear and nonlinear characterization of low-stress high-confinement silicon-rich nitride waveguides: erratum," Opt. Express **25**(7), 7443–7444 (2017).
30. K. J. Ooi, D. K. Ng, T. Wang, A. K. Chee, S. K. Ng, Q. Wang, L. K. Ang, A. M. Agarwal, L. C. Kimerling, and D. T. Tan, "Pushing the limits of CMOS optical parametric amplifiers with USRN:Si_7N_3 above the two-photon absorption edge," Nat. Commun. **8**, 13878 (2017).
31. M. Mitrovic, X. Guan, H. Ji, L. K. Oxenløwe, and L. H. Frandsen, "Four-wave mixing in silicon-rich nitride waveguides," in *Frontiers in Optics*, OSA Technical Digest (online) (Optical Society of America, 2015), paper FM1D.6.
32. G. Wilk, R. Wallace, and J. Anthony, "High-κ gate dielectrics: Current status and materials properties considerations," J. Appl. Phys. **89**(10), 5243–5275 (2001).
33. J. D. Bradley, C. C. Evans, J. T. Choy, O. Reshef, P. B. Deotare, F. Parsy, K. C. Phillips, M. Lončar, and E. Mazur, "Submicrometer-wide amorphous and polycrystalline anatase TiO_2 waveguides for microphotonic devices," Opt. Express **20**(21), 23821–23831 (2012).
34. C. C. Evans, K. Shtyrkova, J. D. Bradley, O. Reshef, E. Ippen, and E. Mazur, "Spectral broadening in anatase titanium dioxide waveguides at telecommunication and near-visible wavelengths," Opt. Express **21**(15), 18582–18591 (2013).
35. M. Hayrinen, M. Roussey, V. Gandhi, P. Stenberg, A. Saynatjoki, L. Karvonen, M. Kuittinen, and S. Honkanen, "Low-loss titanium dioxide strip waveguides fabricated by atomic layer deposition," J. Lightwave Technol. **32**(2), 208–212 (2014).
36. O. Reshef, K. Shtyrkova, M. Moebius, S. Griesse-Nascimento, S. Spector, C. Evans, E. Ippen, and E. Mazur, "Polycrystalline anatase titanium dioxide microring resonators with negative thermo-optic coefficient," J. Opt. Soc. Am. B **32**(11), 2288–2293 (2015).
37. F. Qiu, A. Spring, and S. Yokoyama, "Athermal and high-Q hybrid TiO_2–Si_3N_4 ring resonator via an etching-free fabrication technique," ACS Photonics **2**(3), 405–409 (2015).
38. C. C. Evans, K. Shtyrkova, O. Reshef, M. Moebius, J. D. Bradley, S. Griesse-Nascimento, E. Ippen, and E. Mazur, "Multimode phase-matched third-harmonic generation in sub-micrometer-wide anatase TiO_2 waveguides," Opt. Express **23**(6), 7832–7841 (2015).
39. C. C. Evans, C. Liu, and J. Suntivich, "Low-loss titanium dioxide waveguides and resonators using a dielectric lift-off fabrication process," Opt. Express **23**(9), 11160–11169 (2015).
40. C. Evans, C. Liu, and J. Suntivich, "TiO_2 nanophotonic sensors for efficient integrated evanescent raman spectroscopy," ACS Photonics **3**(9), 1662–1669 (2016).
41. M. Lamy, C. Finot, J. Fatome, J. Arocas, J.-C. Weeber, and K. Hammani, "Demonstration of high-speed optical transmission at 2 μm in titanium dioxide waveguides," Appl. Sci. **7**(6), 631 (2017).
42. J. Park, S. K. Ozdemir, F. Monifi, T. Chadha, S. H. Huang, P. Biswas, and L. Yang, "Titanium dioxide whispering gallery microcavities," Adv. Opt. Mater. **2**(8), 711–717 (2014).
43. T. Kornher, K. Xia, R. Kolesov, B. Villa, S. Lasse, C. S. Sandu, E. Wagner, S. Harada, G. Benvenuti, H.-W. Becker, and J. Wrachtrup, "Amorphous silicon-doped titania films for on-chip photonics," ACS Photonics **4**(5),

Optics EXPRESS

1101–1107 (2017).
44. P. Löbl, M. Huppertz, and D. Mergel, "Nucleation and growth in TiO_2 films prepared by sputtering and evaporation," Thin Solid Films **251**(1), 72–79 (1994).
45. U. D. Dave, B. Kuyken, F. Leo, S. P. Gorza, S. Combrie, A. De Rossi, F. Raineri, and G. Roelkens, "Nonlinear properties of dispersion engineered InGaP photonic wire waveguides in the telecommunication wavelength range," Opt. Express **23**(4), 4650–4657 (2015).
46. D. Milam, "Review and assessment of measured values of the nonlinear refractive-index coefficient of fused silica," Appl. Opt. **37**(3), 546–550 (1998).
47. M. Hemissi and H. A. Adnani, "Optical and structural properties of titanium oxide thin films prepared by sol gel method," Dig. J. Nanomater. Biostruct. **2**(4), 299–305 (2007).
48. S. Friberg and P. Smith, "Nonlinear optical glasses for ultrafast optical switches," IEEE J. Quantum Electron. **23**(12), 2089–2094 (1987).
49. R. Adair, L. L. Chase, and S. A. Payne, "Nonlinear refractive index of optical crystals," Phys. Rev. B Condens. Matter **39**(5), 3337–3350 (1989).
50. K. Ikeda, R. E. Saperstein, N. Alic, and Y. Fainman, "Thermal and Kerr nonlinear properties of plasma-deposited silicon nitride/ silicon dioxide waveguides," Opt. Express **16**(17), 12987–12994 (2008).
51. I. Cristiani, R. Tediosi, L. Tartara, and V. Degiorgio, "Dispersive wave generation by solitons in microstructured optical fibers," Opt. Express **12**(1), 124–135 (2004).

1. Introduction

Efficient photonic integrated circuits (PICs) operating at typical telecommunication wavelengths around 1550 nm are becoming increasingly favorable in many applications ranging from ultra-dense data processing [1] and quantum technologies [2] to metrology [3], optical coherence tomography [4,5] and biomedical sensing [6], which require linear devices, as e.g. optical filters [7–9] and (de)multiplexers [10,11] as well as nonlinear devices, as e.g. ultra-fast all-optical switches [12], wavelength converters [13,14], and multiple wavelength generators [15–19]. When talking about efficiency, compactness and low loss are the two basic requirements. Additionally, large nonlinearity and small nonlinear loss, i.e. energy-effectiveness, are usually also required for the waveguides comprising the devices. Moreover, the materials and fabrication processes for the PICs are highly preferred to be compatible with the complementary metal-oxide-semiconductor (CMOS) technologies matured by the electronics industry to exploit manufacturing scalability.

Unfortunately, the past decades have witnessed very few material platforms for PICs meeting simultaneously the above-mentioned requirements. As to CMOS–compatible photonic waveguides, biggest hopes are anchored to silicon waveguides due to silicon's large refractive index and its capability of integration with silicon-based electronic integrated circuits (ICs). However, because of a small electronic bandgap (1.12 eV) of silicon, two-photon absorption (TPA) and the associated free carrier absorption (FCA) dramatically limit the nonlinear performances of silicon waveguides around 1550 nm [20]. As an alternative, stoichiometric silicon nitride (Si_3N_4) waveguides have been investigated and applied to achieve key nonlinear devices, including octave supercontinuum generators [21] and frequency comb generators [22], thanks to small propagation losses (0.7 dB/cm) and a large bandgap (5 eV). However, the small refractive index of Si_3N_4 (~2.0) yields a large footprint of the photonic devices based on Si_3N_4 waveguides, and the high tensile stress inside thick Si_3N_4 layer may create cracks in the film limiting the ability for dispersion engineering [23]. Resembling Si_3N_4 waveguides, newly reported CMOS-compatible tantalum pentoxide (Ta_2O_5) waveguides also encounter the problem of large dimensions due to a similarly small refractive index of Ta_2O_5 (2.05) in spite of an ultra-low propagation loss [24]. Most recently, silicon-rich nitride (SRN) waveguides have attracted much attention since SRN film can be fabricated with low stress, while possessing a large bandgap as well as having a large refractive index [25–31], by tuning the reactive gas ratios to enrich the silicon concentration. Whereas it is a quite promising platform for PICs, research on SRN waveguides is still in its infancy and some of the deposited SRN material exhibit quite large material losses (7 dB/cm [26]).

Titanium dioxide (TiO_2), well-known as a candidate for high-κ gate dielectrics in memory capacitors and transistors in the CMOS ICs technology [32], is currently inspiring researchers within PICs due to its large refractive index (>2.2) and large nonlinear index being >3 times

Optics EXPRESS

that of Si_3N_4, along with a large TPA-free bandgap (>3.1 eV) at 1550 nm, and a broad transparency window from visible to mid-infrared wavelengths [33–43]. Typically, TiO_2 waveguides have been fabricated, exhibiting linear losses around 5 dB/cm at telecommunication wavelengths (4 dB/cm [33], 5 dB/cm [35], 5.8 dB/cm [36], 4 dB/cm [37]), and TiO_2 photonic devices including directional couplers (DCs) [33] and microring resonators (MRRs) [36,37,39] have also been demonstrated. The quality factors (Q) of the MRRs reaches 1.5 x 10^5 around 1550 nm, however still having large ring radii around 200 μm [37] or 150 μm [39], and not being fully etched ridge waveguides allowing for optimal designs from compact MRRs. Although spectral broadening [34], Raman scattering [40] around 790 nm, and third-harmonic generation [38] for generating visible light have been demonstrated in the TiO_2 waveguides, much work is still to be done to assess the performance of TiO_2 waveguides in a nonlinear process like four-wave mixing at telecommunication wavelengths. Furthermore, considering that previously demonstrated 250nm-thick waveguides showed a nonlinearity of 1.5 W^{-1} m^{-1} at 1565 nm [34], which is only comparable to Si_3N_4, a thicker TiO_2 film could be utilized to confine more light in the TiO_2 core material, hence, increasing the nonlinearity.

In the work presented here, compact TiO_2 waveguides are fabricated and measured, showing a strong confinement to light and a loss of 4-7 dB/cm at telecom wavelengths. A fabricated TiO_2 MRR having a ring radius as small as 50 μm is found to exhibit a loaded Q-value of 53500. Four-wave mixing measurements have been carried out on the waveguides, from which nonlinear parameters of 21-34 W^{-1} m^{-1} are extracted and a wavelength conversion efficiency of −36.2 dB is achieved.

2. Waveguide fabrication and linear characterization

Starting with a thermally grown oxide (~2.4 μm) on a silicon wafer, we deposit the TiO_2 film by using a reaction between oxygen and sputtered titanium metal in an argon/oxygen (Ar_2/O_2) ion beam sputtering machine (Oxford, Ionfab 300). The gas flows used are 9 sccm and 2 sccm for Ar_2 and O_2, respectively, and the sputtering power is 875 W. During the deposition, the silicon wafer is kept at room temperature (20 °C) by using a helium cooling gas, which is supposed to produce an amorphous TiO_2 film according to the previous literature [44]. After 8 hours of deposition, ellipsometry reveals a TiO_2 film thickness of 380 nm. The measured refractive index (n) and the extinction coefficient (k), fitted by the CodyLorentz model, of the deposited film are shown in Fig. 1(a) a as a function of wavelength. At 1550 nm, the refractive index is 2.31 and the film is without significant loss ($k<10^{-5}$) from 570 nm to 1600 nm, which is derived from a large bandgap of ~3.4 eV. Figure 1(b) shows an atomic force microscope (AFM) image of the deposited TiO_2 film and reveals an average surface roughness, R_a, of ~0.4 nm of our amorphous TiO_2 film.

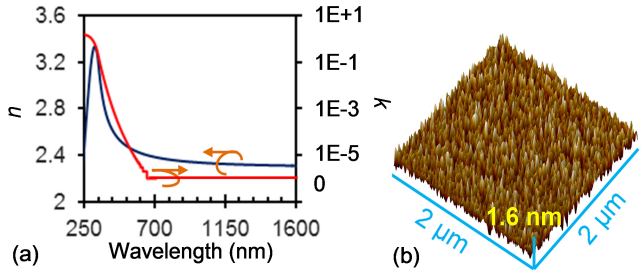

Fig. 1. (a) The measured index (n) and extinction coefficient (k), and (b) an AFM image of the deposited TiO_2 film.

TiO_2 waveguides are fabricated in the deposited film. Firstly, electron-beam (e-beam) lithography is used to pattern the waveguides in an e-beam positive resist (ZEP520A) deposited on the TiO_2 film. By utilizing a metal evaporation and lift-off process, the patterns are subsequently transferred to a 55 nm thick aluminum (Al) film to act as an etching mask

Optics EXPRESS

for the TiO_2. The TiO_2 is dry-etched by using a gas mixture of tetrafluoromethane (CF_4, 20 sccm) and hydrogen (H_2, 10 sccm) gasses. The residual Al mask is stripped from the TiO_2 waveguides and no cladding is covered on the top. Figure 2(a) shows a scanning electron microscope (SEM) image of the cross section of a fabricated TiO_2 waveguide. The shape of the waveguide with height h = 380 nm is trapezoidal with base width w_1 and top width w_2 resulting in sloped sidewalls with angles $\theta = 73°$. The waveguides are slightly over etched by h_{in} = 75 nm into the buried oxide layer. Figures 2(b) and 2(c) show the calculated field distributions of the fundamental transverse-electric (TE) mode and the transverse-magnetic (TM) mode, respectively, of a TiO_2 waveguide with w_1 = 1150 nm. Here, an eigenmode solver, (Mode Solution from Lumerical Solutions) is used and the wavelength is 1550 nm. In the figures, the effective index (n_{eff}), the effective mode area (A_{eff}) and the power ratio confined in the TiO_2 (Γ_{TiO2}) are also given. Due to a relatively large thickness of the TiO_2, both the TE- and TM-modes are tightly confined in the TiO_2 with the TE mode having the higher confinement (Γ_{TiO2} = 81%). The strong confinement will not only allow for compact footprints of the TiO_2 photonic devices in general but will also enhance the nonlinear performances of the TiO_2 waveguides.

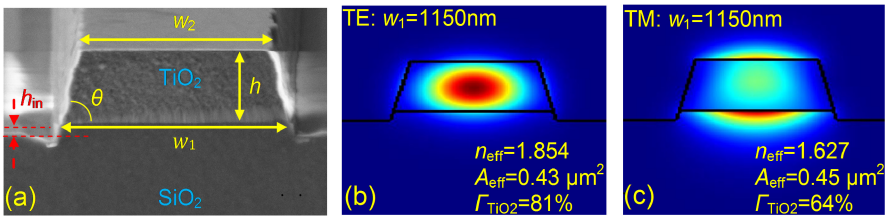

Fig. 2. (a) SEM image of a fabricated TiO_2 waveguide. The calculated field distributions of the TE- (b) and TM- (c) modes in a TiO_2 waveguide with w_1 = 1150 nm at wavelength 1550 nm.

Using a cut-back method, we have measured the propagation loss of the fabricated waveguides and the coupling losses to a tapered and lensed fiber. Figure 3(a) shows the normalized transmission measured at 1550 nm for different lengths of waveguides having w_1 = 1150 nm for the TM- (red triangles) and the TE-modes (blue dots). Also shown are measurements for TE-polarized light in a waveguide having w_1 = 1630 nm (green squares). Linear fittings for each set of measurements are also given. All the measured transmissions are normalized to a fiber-to-fiber measurement to exclude the influence of the setup. For a given width and length, 4 or 5 identical waveguides are fabricated and measured to estimate the uncertainty and process variations. The propagation loss α for the TE mode in the waveguide with w_1 = 1150 nm is found to be 5.4 ± 1.0 dB/cm, which is larger than the loss of the TM mode (4.1 ± 0.9 dB/cm) in the same waveguides since the TM mode has less overlap with the slightly rough sidewalls. The wider waveguides with w_1 = 1630 nm generally has a lower propagation loss (5.0 ± 1.6 dB/cm) when the light is TE- polarized due to a lower overlap with the sidewalls in the wider waveguides. Figure 3(b) shows the propagation loss and the coupling loss as a function of wavelengths ranging from 1500 nm to 1580 nm for the TE mode in a waveguide with w_1 = 1150 nm. Generally, the propagation loss is 4-7 dB/cm and the coupling loss is ~8 dB per facet (8.0 ± 0.6 dB at 1550 nm). The large coupling loss is due to a strong confinement of the waveguide compared to the lensed fiber, and can be reduced by introducing an inverse waveguide taper scheme to more efficiently couple light from the lensed fibers to the waveguides.

Optics EXPRESS

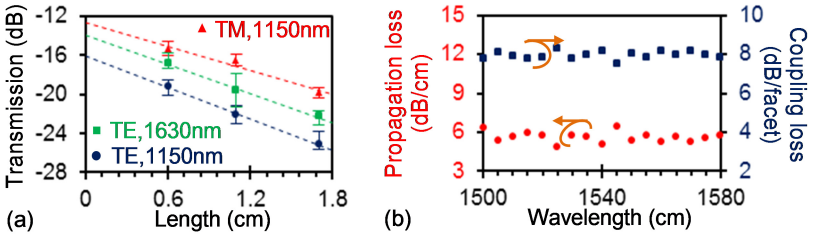

Fig. 3. (a) Transmission as a function of the waveguide length for the fabricated TiO_2 waveguides with different widths and for different polarizations at wavelength 1550 nm. Linear fittings are given as dashed lines. (b) The propagation loss (red circles) and coupling loss (blue squares) at different wavelengths in the waveguide with w_1 = 1150 nm for the TE mode.

Microring resonators (MRRs) with a compact footprint and a high quality factor are key components in passive photonic integrated circuits and for several nonlinear applications like high-efficiency frequency comb generation [19]. The high index contrast between the TiO_2 core and its surroundings (i.e. silica and air) and the large thickness of our waveguides produce a strong confinement of light propagating in the waveguide and facilitate compact TiO_2 MRRs. To verify this, we have fabricated and characterized MRRs having waveguide widths w_1 = 1150 nm and bending radii R = 50 μm but designed with different coupling gaps between the ring and the bus waveguide. Figure 4(a) shows the measured and normalized spectrum for TE-polarized light in an MRR with a coupling gap of 300 nm. From the spectrum, a group index n_g of 2.568 can be extracted from a free spectral range (FSR) of 2.982 nm and agrees well with the theoretical value of 2.536 calculated by using $n_g = \lambda^2/(2\pi \bullet R \bullet FSR)$, where λ = 1550.894 nm. A zoom-in around the resonance at 1550.894 nm is shown in Fig. 4(b) where a Lorentzian curve (green line) is used to fit the measured spectrum (blue dot). From the fitted curve, a full-width at half-maximum (FWHM) of 29 pm is extracted resulting in a loaded Q-factor (Q_{load}) of ~53500. With the coupling gap of 300 nm, the MRR is under-coupled and the intrinsic Q-factor Q_{int} can be calculated as ~73500 according to [37],

$$Q_{int} = \frac{2Q_{load}}{1+\sqrt{T_0}} \quad (1)$$

where T_0 (= 0.207) is the transmission normalized to the maximum value of the fitting curves at the resonant wavelength (λ_0 = 1550.894 nm). Knowing the radius R and the FSR of the MRR, the waveguide loss of the ring α_{ring} can be calculated by $\alpha_{ring} = 2\pi n_g/(Q_{int} \bullet \lambda_0)$ giving a loss of 6.1 dB/cm, which is slightly higher than the measured loss of the straight waveguide (5.4 ± 1.0 dB/cm) due to a larger mode overlap with the sidewalls in the bent waveguide.

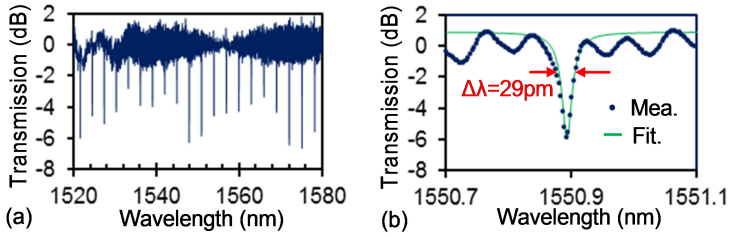

Fig. 4. (a) Measured and normalized transmission spectrum of a TiO_2 MRR with a radius of 50 μm. (b) Enlarged spectrum (blue dots) and the Lorentzian fitting curve (solid green) at the resonant wavelength around 1550.894 nm.

Optics EXPRESS

3. Nonlinear characterization

Figure 5 shows the experimental setup for performing four-wave mixing (FWM) experiments in the fabricated straight TiO_2 waveguides. The pump and probe signals from two continuous wave (CW) lasers are separately polarized by a polarization controller (PC), amplified by a erbium-doped fiber amplifier (EDFA), filtered by a 1-nm band-pass filter, and then combined in a ratio 10:1, respectively, by using a 10 dB fiber coupler. After passing through a polarization beam splitter (PBS) and another PC, the two signals are injected into the TiO_2 waveguides by using a tapered and lensed fiber. Here, the PBS is used to switch between the TE and TM polarizations. The output light from the waveguides is collected by another tapered and lensed fiber and analyzed by an optical signal analyzer (OSA). In order to monitor the input and output powers of the waveguides, two power meters are connected via two 20 dB fiber couplers positioned before and after the waveguides.

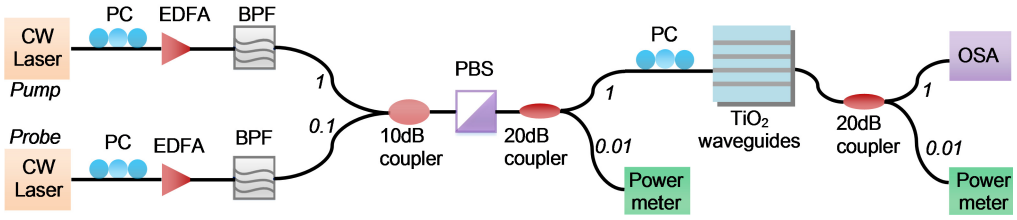

CW: *continuous wave;* PC: *polarization controller;* EDFA: *erbium-doped fiber amplifier;* BPF: *band-pass filter;* PBS: *polarization beam splitter;* OSA: *optical spectrum analyzer*

Fig. 5. Experimental setup for performing FWM experiments in the fabricated TiO_2 waveguides.

During the measurements, we fix the wavelengths of the pump and the probe to 1550.1 nm and 1551.3 nm, respectively. We have measured the output FWM spectra for the TE mode and the TM mode in a TiO_2 waveguide with the width w_1 = 1150 nm and the length L = 1.1 cm when the power of the input probe signal is fixed at 12.7 dBm but varying the power of input pump signal. Figure 6(a) shows the spectra for the maximum input pump power used (27.8 dBm/27.6 dBm) for the TE/TM (blue/red) mode, respectively. From the spectra, one can extract the FWM conversion efficiencies (CEs) of −36.2 dB and −37.2 dB for the TE mode and the TM mode, respectively, with the CE defined as the ratio of the output idler power to the output probe signal power. Furthermore, the nonlinear parameter γ can be calculated by [45],

$$CE=(\eta P_{\text{pump}} L_{\text{eff}} \gamma)^2 \qquad (2)$$

where P_{pump} is the coupled pump power being the input pump power minus the fiber-waveguide coupling loss and L_{eff} is the effective interaction length of the pump and probe signal in the waveguide defined as $(1\text{-}e^{-\alpha L})/\alpha$, where L is the length of the waveguide with propagation loss α. We reasonably assume that γ is real since no TPA is present at the wavelengths in focus due to a large measured bandgap (3.4 eV). Moreover, we assume that η = 1 since the phase mismatch is negligible for the small spectral separation between the pump and the probe signals. Figure 6(b) shows the calculated CEs with respect to the different coupled pump powers for the TE (blue square) mode and the TM (red circle) mode along with quadratic fittings (dashed lines) when using the maximum value of the coupling losses, i.e. the highest nonlinear efficiency. The quadratic fittings are in very good agreement with the measured values which supports the assumption of neglecting TPA effects. The highest value of the nonlinear parameter γ can be extracted to 34 W^{-1} m^{-1} and 19 W^{-1} m^{-1} using the maximum values of the propagation loss in the calculations for the TE mode and the TM mode, respectively. The measured nonlinearity of the TE mode is almost twice as large as that of the TM mode since the TE mode is more confined in the TiO_2 core. The lowest value of γ can be calculated by using the minimum values of the coupling loss and the propagation loss

Optics EXPRESS

in the calculations resulting in nonlinear parameters γ of 21 W^{-1} m^{-1} and 14 W^{-1} m^{-1} for the TE mode and the TM mode, respectively. Knowing the waveguide dimensions and the calculated nonlinear parameters, it is easy to calculate the effective nonlinear refractive index ($n_{2,\text{eff}}$) of the TiO_2 waveguide as $n_{2,\text{eff}} = (\gamma\lambda A_{\text{eff}})/(2\pi)$. Using the parameters of the TE mode and the lowest and the highest values of γ, $n_{2,\text{eff}}$ is calculated to be 2.3-3.6 x 10^{-18} m^2/W. Although both the TiO_2 core and the buried silica layer contribute to the nonlinearity of the waveguides, the contribution of the silica layer is smaller than 0.2% due to a low refractive index (1.444), a low power ratio in this layer (Γ_{silica}~11%) as well as a quite low nonlinear refractive index of silica (~0.028 x 10^{-18} m^2/W [46]). Consequently, the calculated $n_{2,\text{eff}}$ is almost equal to the nonlinear refractive index of the deposited TiO_2 material, which is one order of magnitude larger than that of Si_3N_4 and approximately half the value of that of silicon.

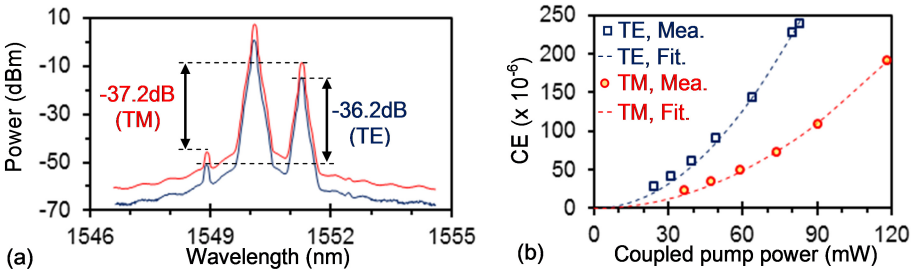

Fig. 6. FWM spectra for the TE- (blue) and TM- (red) modes in a waveguide with w_1 = 1150 nm and L = 1.1 cm for the maximum input pump powers. (b) The conversion efficiency (CE) with respect to different coupled pump powers for both the TE- (blue) and TM- (red) modes.

4. Discussion

The nonlinear index n_2 (2.3-3.6 x 10^{-18} m^2/W at 1.55 μm) of our deposited TiO_2 material is consistent with reported values at near infrared wavelengths (~1.6 x 10^{-18} m^2/W [47], 2.0 x 10^{-18} m^2/W [48], and ~3.6 x 10^{-18} m^2/W [49]), and is 1~2 orders of magnitudes larger than that of silicon nitride (0.24 x 10^{-18} m^2/W [50]) and silica (~0.028 x 10^{-18} m^2/W [46]). However, to the best of our knowledge, our results successfully verify for the first time the high nonlinear index of TiO_2 used for realizing compact waveguides. TiO_2 waveguides have already been demonstrated for spectral broadening, but the extracted n_2 (0.16 x 10^{-18} m^2/W) is relatively small [34]. Furthermore, due to a larger waveguide height of 380 nm, our waveguides confine 81% of power in the TiO_2 core and correspondingly enhance the nonlinearity of the waveguide to 21-34 W^{-1} m^{-1}. This is an order of magnitude larger than previously demonstrated waveguides confining ~60% of the power in a 250nm-high TiO_2 core [34].

Anomalous dispersion is usually needed to achieve key nonlinear processes like supercontinuum generation [21, 51]. Having a thicker waveguide core, i.e. having a larger mode confinement in the core, may simplify the dispersion engineering. Figure 7 shows the calculated dispersion D as a function of wavelengths for the TE mode in a TiO_2 waveguide with w_1 = 1150 nm and thicknesses of 250 nm (green line), 380 nm (red line) and 400 nm (blue line). From the curves, one can find that the dispersion of the thinner waveguide (250 nm) is away from the anomalous dispersion regime around 1550 nm. In contrast, the 380nm-thick TiO_2 waveguide is close and can easily be tuned to have anomalous dispersion (D>0) in a broad wavelength region by increasing slightly the thickness of the waveguide to 400 nm. This re-depositing of 20 nm TiO_2 on the fabricated waveguides can be achieved by using either sputtering or atomic layer deposition (ALD). The latter can provide an even more accurate control of the re-deposition and can also be used to smoothen the waveguide sidewalls to decrease the propagation loss [35].

Optics EXPRESS

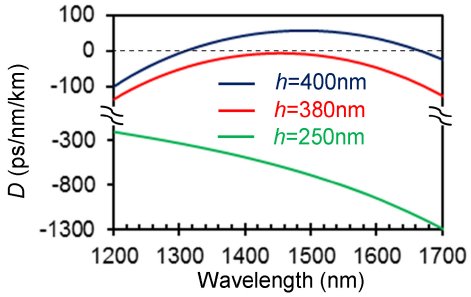

Fig. 7. The wavelength-dependent dispersion for TiO_2 waveguides with the different thickness. Here, the waveguide width is w_1 = 1150 nm and the dashed line shows the zero dispersion.

5. Conclusion

In conclusion, we have fabricated compact TiO_2 waveguides and characterized their linear and nonlinear performances. The waveguides possess a strong confinement of light due to a large refractive index, a thick film of the deposited titanium dioxide and also a full etching for a stripe configuration. Such a strong confinement not only benefits the compactness of the devices but also plays an important role for achieving a high nonlinearity. The contemporary fabrication processes produce a propagation loss of 5.4 ± 1 dB/cm and 4.1 ± 0.9 dB/cm for the TE mode and the TM mode, respectively, which is comparable with that in the previous literatures but may be further decreased by optimizing the processes, including using a resist mask instead of the rough metal mask and tuning the gas ratio in the etching to achieve a more chemical (i.e. softly) etching. Microring resonators have been fabricated and measured to have a moderately large loaded Q (53500) in a compact footprint. Four-wave mixing experiments have been carried out in the TiO_2 waveguides and a conversion efficiency of −36.2 dB can be achieved without the presence of detrimental TPA effects. From the FWM experiments, the nonlinear parameters of the fabricated TiO_2 waveguide and the nonlinear index of the TiO_2 material are calculated to 21-34 W^{-1} m^{-1} and 2.3-3.6 x 10^{-18} m^2/W, respectively. These results, especially the high nonlinearity, pave a promising way for TiO_2 waveguides to be applied in photonic integrated circuits simultaneously having good linear and nonlinear performances and retaining CMOS-compatibility in the fabrication.

Funding

VILLUM Fonden ‘ONCHIP’ Project (VKR023112); Danish National Research Foundation SPOC Research Center of Excellence (DNRF123).

Acknowledgments

We thank Yi Zheng for help on the AFM and DTU Danchip for the support of the fabrication facilities and technologies.